

Experimental Investigation of a Porous Evaporator for a Heat Pipe-Based DEMO Divertor Target Concept

Wen Wen¹, Bradut-Eugen Ghidersa¹, Wolfgang Hering¹, Jörg Starflinger, and Robert Stieglitz

Abstract—Heat pipes can effectively transport heat from a heat source to a heat sink by means of phase transitions of the working fluid inside and capillary forces. Because of their high effective conductivity, they are under consideration for the DEMO in-vessel plasma-facing components. With proper condenser length, heat pipes can enlarge the heat transfer area to the cooling circuit, thus relaxing the requirements for the cooling circuit. The reduced fluid inventory of the heat pipe would also limit the amount of liquid released in case of damage or accidents compared to an actively cooled plasma-facing component, thus increasing the reactor's safety. Recent engineering studies indicate that it is possible to design a water-based heat pipe with mixed capillary structures (axial grooves at the condenser and adiabatic zones and sintered porous material at the evaporator) that would have a capillary driving force large enough to transport an amount of heat corresponding to an applied heat flux of 20 MW/m². However, to validate the design for such high heat fluxes, the capability of the evaporator to withstand such loads should be investigated first. Hence, a dedicated experiment focusing on the performance of the proposed heat pipe evaporator was designed. The experimental results show the operating characteristics of two different evaporator designs: one with a porous structure and one with channels on the porous surface. The influence of liquid inventory and heat sink flow rates on the heat pipe performance are also discussed here.

Index Terms—Heat pipe, high heat flux, plasma facing components, wick porous.

I. INTRODUCTION

THE DEMO divertor targets are usually exposed to high heat fluxes of 10 MW/m², even reaching 20 MW/m² for short periods of time. The EU-DEMO baseline concept uses CuCrZr cooling pipes having W-blocks as protecting armor [1]. However, the heat loading conditions limit the

heat transfer to roughly one third of the pipe's circumference requiring high coolant velocities and the use of a swirl flow for achieving the required performances.

To address these issues, heat pipe technology is seen as an advanced option, which has high-effective heat conductivity. Its condenser area to the external cooling system can be increased, relaxing some of the baseline requirements.

Liquid metal heat pipe is first suggested by Carlson and Hoffman [2] and Schwertz and Hoffman [3] to cool a pool of liquid lithium in the blanket of a tandem mirror fusion reactor and by Kovalenko et al. [4] for the first wall. However, Makhankov et al. [5] found that the transverse magnetic field can profoundly affect the performance of liquid metal heat pipes. Then, it was thought that water-based heat pipes could manage heat fluxes up to 2 MW/m² for plasma-facing components [6], but due to the heater's limitation, the maximum radial heat flux reached is 0.525 MW/m². As such, the water heat pipes never experienced an operating limit.

Due to the lack of research on the use of heat pipes in the DEMO divertor and the uncertain performance of water heat pipes under high heat flux conditions, a divertor target concept based on the water heat pipe was proposed [7].

This new concept, called divertor heat pipe (DIV-HP), uses water as a working liquid. The capillary structures of the DIV-HP use a combination of axial grooves (enclosed by a mesh screen) at the condenser and adiabatic zones and a sintered porous structure at the evaporator [7]. The engineering analysis method employed to dimension the DIV-HP shows that most of the operating limits of DIV-HP are superior to a supposed heat flux of 20 MW/m².

However, there are less precise estimates for the boiling limits, occurring mostly on the evaporator. The spherical evaporator with sintered porous material will receive high heat fluxes, so that the nucleate boiling occurs easily. According to the Afgan study [8], enlarged meniscus surface boundaries in the porous core and vapor channels in the porous structure could raise critical heat fluxes of boiling limit than pool boiling case. However, too many bubbles in the porous structure may disrupt the condensed water that flow back to the evaporator and rewets the hot areas, leading to a rapid temperature increase or dry-out, and the heat pipe will no longer work.

Hence, the boiling behavior in the evaporator porous structure is a critical issue. To address it, an experiment was selected that concentrated solely on the boiling limit at first, particularly the evaporator's performance. According to this purpose, the experimental mock-up heat pipe

Manuscript received 2 October 2023; revised 3 January 2024; accepted 21 February 2024. This work was supported by EUROfusion Consortium, through the European Union via the Euratom Research and Training Program within the framework under Grant 101052200-EUROfusion. The review of this article was arranged by Senior Editor R. Chapman. (Corresponding author: Wen Wen.)

Wen Wen, Bradut-Eugen Ghidersa, Wolfgang Hering, and Robert Stieglitz are with the Institute for Neutron Physics and Reactor Technology, Karlsruhe Institute of Technology, 76344 Eggenstein-Leopoldshafen, Germany (e-mail: wen.wen@kit.edu; bradut-eugen.ghidersa@kit.edu; wolfgang.hering@kit.edu; robert.stieglitz@kit.edu).

Jörg Starflinger is with the Institute of Nuclear Technology and Energy Systems, University of Stuttgart, 70569 Stuttgart, Germany (e-mail: joerg.starflinger@ike.uni-stuttgart.de).

Color versions of one or more figures in this article are available at <https://doi.org/10.1109/TPS.2024.3371572>.

Digital Object Identifier 10.1109/TPS.2024.3371572

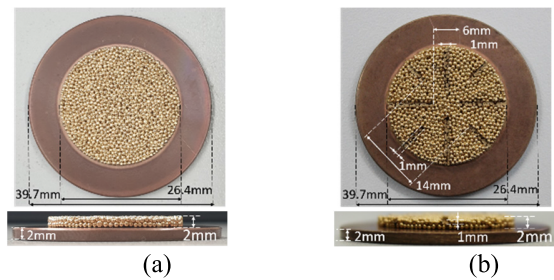


Fig. 1. Porous structure on CuCrZr plate. (a) HPEE-1 with original shape. (b) HPEE-2 with channels.

for evaluating an evaporator (HPEE) was created, as is explained in [9].

The present contribution mainly focuses on the experimental results of two HPEE mock-ups, both of which use the same porous structure, but having different evaporator geometries. A particular attention is given to the impact of the liquid inventory and of the external cooling characteristics.

II. EXPERIMENTAL MOCK-UP DESIGN AND LAYOUT OF THE EXPERIMENTAL SETUP

The design of the HPEE and the experimental setup are discussed in detail in [9]. To facilitate the understanding of the experimental results, the most relevant aspects, especially the evaporator, are briefly summarized in the following.

A. HPEE Mock-Up Design

Two HPEEs with distinct geometries of the evaporator porous structure are studied. They use the same sintered porous material with a particle size of about $400 \mu\text{m}$ and a porosity of 0.47. The only difference is that HPEE-1 has a plain surface and a uniform thickness of 2 mm, as shown in Fig. 1(a), while HPEE-2 has additionally a pattern of channels carved on its surface, as shown in Fig. 1(b). The presence of the channels on the porous structure is intended to reduce the resistance for the bubble to escape when boiling occurs in the porous core, avoiding rewetting of the respective area [10].

For both HPEEs, CuCrZr selected for DIV-HP is adopted for the HPEE envelop. The HPEEs are designed to operate vertically to have a capillary limit well superior to the targeted heat flux (20 MW/m^2), as indicated in Fig. 2. The condenser surface is larger than evaporator surface to increase the contact area with the external coolant. The cylindrical vapor space above the evaporator has a diameter of 25 mm, and the porous structure has a diameter of 26.4 mm to maintain a good similarity to the DIV-HP design. Then, condensed water enters the evaporator porous structure through grooves that are 20 mm long. The porous structure is brazed on a 2-mm-thick CuCrZr plate with a diameter of 39.7 mm, which is protected by a 2-mm tungsten plate. It is similar to the one selected for the DIV-HP. Due to manufacturing issues, the HPEEs use bronze CuSn10(10% tin and 90% copper), rather than the original design that is with copper.

The main dimensions of the HPEEs are listed in Table I.

B. HPEE Mock-Up Instrumentation

Due to space and continuous fluid flow considerations, only the temperatures at HPEE's various locations are monitored

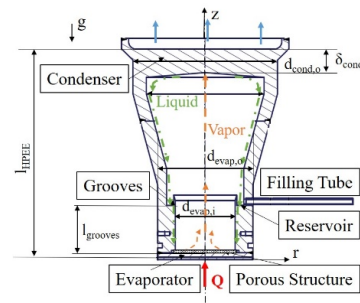


Fig. 2. Cross section of the HPEE mock-up with dimensions.

TABLE I
HPEE GEOMETRY DIMENSIONS

Components of the HPEE	Symbol	Dimensions
Length of the HPEE	l_{HPEE}	88.5mm
Outer diameter of condenser	$d_{\text{cond,o}}$	60.3mm
The thickness of the condenser (CuCrZr)	δ_{cond}	10mm
The outer diameter of the evaporator	$d_{\text{evap,o}}$	39.7mm
The inner diameter of the evaporator	$d_{\text{evap,i}}$	25mm

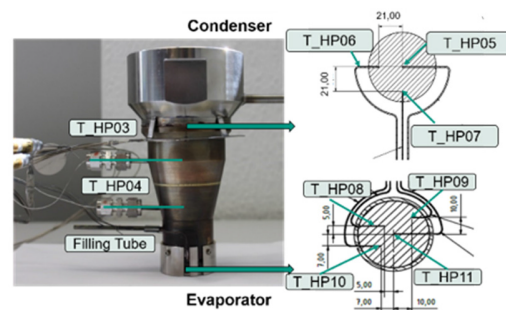


Fig. 3. HPEE's thermocouples for temperature measurements: at condenser (T_HP05-HP07), at vapor thermocouples (T_HP03&HP04), and at evaporator (T_HP08-HP11).

with K-type thermocouples (nominal accuracy $\pm 1.5 \text{ }^\circ\text{C}$ or $\pm 0.4\% T$). Thus, three thermocouples (T_HP05, T_HP06, and T_HP07) are positioned 5 mm below the condenser's surface, as shown in Fig. 3. Two thermocouples (T_HP03 and T_HP04) monitor the vapor temperature in the axial direction. One is 20 mm above the evaporator surface and the other one is 7 mm below the inner condenser surface. Between the evaporator CuCrZr plate and the tungsten one, four thermocouples are installed to measure the wall temperature close to the evaporator: one (T_HP08) placed in the middle and the other three spaced 5, 7, and 10 mm from the center.

C. Experimental Setup

The experiment was performed in a vacuum ($1.6e^{-2}$ mbar) to limit the thermal losses due to heat convection (in the air) and protect the heated surface from unwanted oxidation. The heat loading was provided by the electrically heated copper block. As the power losses to the surroundings were challenging to quantify, the power transferred by the HPEE was evaluated calorimetrically using the temperature, pressure, and flow rate measurements of external coolant's inlet and outlet [9].

TABLE II
LIQUID INVENTORIES FOR DIFFERENT HEAT LOAD RANGES

Heat load range	Liquid inventory	Filling ratio %
0-1MW/m ²	1.5ml	2.0
1-5MW/m ²	1.7ml	2.2
5-20MW/m ²	2.0ml	2.6

The transient calorimetric power is estimated as follows:

$$Q = (h(T_{\text{out}}, p_{\text{out}}) - h(T_{\text{in}}, p_{\text{in}})) * \dot{m}_{\text{out}}(T_{\text{out}}, p_{\text{out}}) \quad (1)$$

where h is the specific enthalpy [J/kg], and $\dot{m}_{\text{out}}(T_{\text{out}}, p_{\text{out}}) = \rho(T_{\text{out}}, p_{\text{out}}) * \dot{V}_{\text{out}}$, ρ is the coolant density [kg/m³]. Both quantities are calculated based on the provisions of IAPWS Industrial Formulation 1997 for Region 2 [11].

The uncertainties of the average experimental measurements and calorimetric power at steady state are analyzed according to the Taylor Series and GUM [12]

$$u_{em} = \frac{1}{n} \sqrt{(u_{em1}^2 + u_{em2}^2 + \dots + u_{emn}^2)} \quad (2)$$

where n is the number of the repeated test. $u_{emn} = ((b_{emn}^2 + s_{emn}^2))^{1/2}$. b_{emn} is the systematic uncertainties based on the sensor's accuracy [9] and the resolution of measurement equipment. s_{emn} are the random standard uncertainties based on the measurements' stand deviation.

D. Experimental Procedure

The testing of the HPEE increases the applied heat flux gradually from 0.2 MW/m². Given the wide range of the surface heat fluxes, the evaporation rate changes significantly and, consequently, the amount of water needed for the heat pipe operation [13]. If the water amount is set for the highest load level (here 20 MW/m²), it leads a flooded evaporator at low heat flux, and pool-boiling dominates the heat pipe operation. Hence, for HPEE, the water inventory, as well as the filling ratio (Water amount/Vapor space), increased progressively with test heat fluxes, as indicated in Table II. This allows us to focus the investigation on the performances of the evaporator with the phase change occurring at the porous structure. For each selected heat flux range, a small reservoir over the grooves retains the condensed water excess.

To study the influence of the external cooling characteristics on the HPEE evaporator performance, three heat sink flow conditions are choose as follows.

- 1) Flow rate (90l/h) maintained when increasing heat flux, to ensure the high accuracy of the measurements and the temperature rise of the coolant, minimizing the relative uncertainty of the calorimetric power at low tested heat flux from 0.2 to 2 MW/m².
- 2) Flow rate adjusted to keep the coolant temperature rise around 8 °C from heat flux of 2 MW/m², to keep relative uncertainty low as well.
- 3) Flow rate is controlled to keep the condenser temperature at 83 °C, to see the influence of the condenser temperature on the evaporator.

Each HPEE was put in a starting water volume of 1.7 mL by a scaled syringe (0.2-mL water is needed for pushing out gas and filling the feeding connections and tube before the liquid

is sent into the HPEE; 1.5-mL water is required by HPEE operation). The first flow rate is set to 90l/h. Its performance was assessed by stepping up the heat flux from 0.2 MW/m² with an average jump of 0.2 MW/m². Until the HPEE shows the signs of unstable operation or meets the operation limits, the flow rate increased to level "2," and the applied heat flux is started from 2 MW/m² directly. After the HPEE meets the operation limits again, repeat the test with flow rate "3" from 2 MW/m². After the test with 1.5-mL liquid meets its limit at all flow rate levels, the water amount needed by HPEE was increased to 1.7 and 2.0 mL, and the investigation repeated.

III. RESULTS

The HPEE's heat transfer capabilities, mainly focusing on the performance of the evaporator, are evaluated by examining the boiling curves of the HPEE and the temperature difference between the evaporator and condenser.

A. Influence of the Liquid Inventories on HPEEs

The heat transfer of the heat pipe occurs via two pathways [14]: 1) conduction through the capillary and wall and 2) the latent heat transported from the evaporator to the condenser by two-phase change process through the convection of the vapor flow. Because a two-phase change process has a higher effective conductance than the wall and the capillary structure, during a two-phase change operation, the temperature difference between the evaporator and condenser $\Delta T_{\text{evap-cond}}$, in which T_{evap} is the average value of T_HP08, T_HP09, T_HP10, and T_HP11 on the evaporator and T_{cond} is the average value of T_HP05, T_HP06, and T_HP07 in the condenser, is lower than one only through wall conduction.

To compare them, one conduction-only model is built, which estimated temperature difference between evaporator and condenser by Fourier's law: $Q = -\lambda A(dT/d\delta)$, where Q is the power, transferred only through the HPEE envelop and capillary structure with heat conductivity λ . A is the heat transfer surface, and δ is the thickness.

Fig. 4 shows the temperature difference between the evaporator and condenser of the two HPEEs as a function of the heat flux by considering different water filling ratios and compared with the conduction-only model. At low heat fluxes (up to 0.2 MW/m²), the heat transfer of HPEE-1, featuring a plain evaporator, seems to be dominated by conduction, as the measures temperature difference equals the conduction only model. When heat fluxes are between 0.2 and 0.4 MW/m², the temperature difference remains unchanged and is independent of the water content. Above 0.4 MW/m², the $\Delta T_{\text{evap-cond}}$ dependence on the heat flux for HPEE-1 is linear and below the value of the conduction-only model, meaning that the heat transport is dominated by a heat-pipe effect, and the slopes reduce when water content increases. For HPEE-2 with channels on the grooves, the measured temperature difference is always lower than the case of conduction only. The maximum relative low uncertainty of $\Delta T_{\text{evap-cond}}$ is 2.5% in the entire test range for both HPEEs.

At 0.4 MW/m², the temperature difference between the evaporator and condenser $\Delta T_{\text{evap-cond}}$ of HPEE-1 with the lowest amount 1.5 mL jumped from 46 °C ± 0.7° to 65 °C

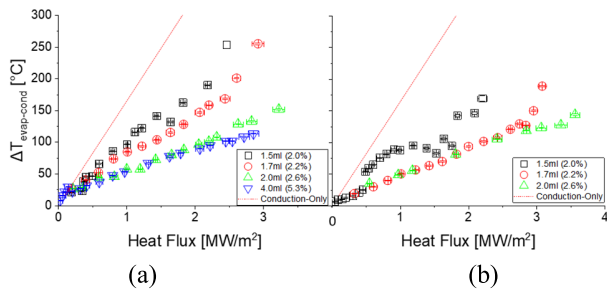


Fig. 4. Comparison of the temperature difference between evaporator and condenser for a given transferred heat flux and liquid inventories with “flow 90 L/h.” (a) HPEE-1 and (b) HPEE-2.

± 0.8 °C in Fig. 4(a), because the boiling regime changed, resulting a reduction of the HPEE’s effective thermal conductivity. Then, up to 2.5 MW/m^2 , the temperature difference jumps again from $191 \text{ °C} \pm 1.1 \text{ °C}$ to $252 \text{ °C} \pm 1.6 \text{ °C}$. When liquid inventory increased to 1.7 mL, $\Delta T_{\text{evap-cond}}$ of HPEE-1 only showed a jump at 2.6 MW/m^2 . The test was continued at 3 MW/m^2 , where $\Delta T_{\text{evap-cond}}$ reached $253 \text{ °C} \pm 1.5 \text{ °C}$, of which the evaporator temperature reached $380 \text{ °C} \pm 1.4 \text{ °C}$. Then, the $\Delta T_{\text{evap-cond}}$ of the HPEE-1 with liquid inventories of 2.0 and 4.0 mL increased linearly with heat flux without a jump. The final $\Delta T_{\text{evap-cond}}$ of HPEE-1 with 2.0 mL was $151.8 \text{ °C} \pm 0.8 \text{ °C}$ at 3.2 MW/m^2 , and $\Delta T_{\text{evap-cond}}$ with 4.0 mL was around $100 \text{ °C} \pm 0.7 \text{ °C}$ at 2.8 MW/m^2 . Because the evaporator temperature was close to 350 °C and the electric copper heater was close to its working temperature limit of 750 °C , the experiments were stopped.

In comparison, $\Delta T_{\text{evap-cond}}$ of HPEE-2 with 1.5 mL showed a clear jump from $24 \text{ °C} \pm 0.72 \text{ °C}$ to $54 \text{ °C} \pm 0.68 \text{ °C}$ at 0.5 MW/m^2 in Fig. 4(b). Then, it fluctuated around $90 \text{ °C} \pm 1.8 \text{ °C}$ in a specific heat flux range and suddenly jumped directly from $95 \text{ °C} \pm 2.4 \text{ °C}$ to $140 \text{ °C} \pm 3.1 \text{ °C}$ at 1.8 MW/m^2 . $\Delta T_{\text{evap-cond}}$ of HPEE-2 containing 1.7-mL water showed a jump at 2.9 MW/m^2 , which is higher than the heat flux at one with HPEE-1. Compared with the HPEE-1, $\Delta T_{\text{evap-cond}}$ with 2.0 mL was $127 \text{ °C} \pm 1.1 \text{ °C}$ at 3.2 MW/m^2 , lower than HPEE-1 with 2.0 mL by 25 °C . The experiments stopped at 3.6 MW/m^2 due to the copper heater limit. No dry-out is overserved through entire experiments.

Both HPEEs show a potential to accept more heat flux, as the curve is still linear without a suddenly unstable rise at the end of experiments. When applied same heat flux, the temperature difference of HPEE-2 is lower than HPEE-1 because the porous structure’s thickness where the channels are is half as compared to HPEE-1, resulting a lower effective heat resistance, and the water evaporation and vapor convection are initiated easily than in HPEE-1.

The heat transfer performance of the HPEE evaporator is characterized by studying the boiling curves related to the heat flux and superheat $\Delta T_{\text{wall-HP04}}$ of the tested evaporator [15]. T_{wall} is the temperature of interface between the evaporator CuCrZr plate and the porous structure, calculated from the average value of the four thermocouples on the evaporator by assuming a uniform heat flux distribution through the CuCrZr plate. While T_{HP04} is the vapor temperature measured by T_{HP04} , which is 20 mm away from the porous surface, as the vapor temperature variation is low in the axial direction.

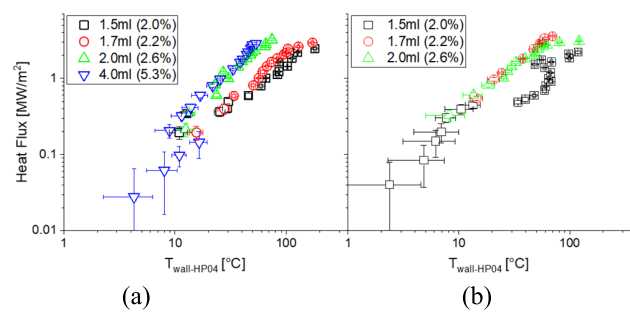


Fig. 5. Boiling curves of two mock-ups with different liquid inventories with “flow 90 L/h.” (a) HPEE-1 and (b) HPEE-2.

Fig. 5 shows the boiling curves of the two HPEEs investigated by considering different water filling. For HPEE-1, in the case with 1.5-mL liquid, when the heat flux is around 0.2 MW/m^2 , $\Delta T_{\text{wall-HP04}}$ is $10 \text{ °C} \pm 2.0 \text{ °C}$, as in Fig. 5(a). When the heat flux increased to 0.4 MW/m^2 , the boiling curve shifts to the right. $\Delta T_{\text{wall-HP04}}$ rises from $12 \text{ °C} \pm 1.4 \text{ °C}$ to $25 \text{ °C} \pm 2.8 \text{ °C}$ with relative high uncertainty of 10%. Then, the boiling curve increases linearly. This shift in the boiling curve is interpreted as a change in the boiling regime. At 2.2 MW/m^2 , the superheat is $130 \text{ °C} \pm 1.6 \text{ °C}$ with relative uncertainty of 1.2%, after which $\Delta T_{\text{wall-HP04}}$ increased rather quickly, but heat flux changed little, meaning the slope of the curve became mild. It indicates a sign of the boiling regime shifting again. For a liquid inventory of 1.7 mL, the superheat $\Delta T_{\text{wall-HP04}}$ of HPEE-1 increases linearly as a function of heat flux up to 2.4 MW/m^2 , and the slopes became gentle. When water inventory is 2 mL, $\Delta T_{\text{wall-HP04}}$ has lower values than those recorded for a water inventory of 1.7 mL. The curve increases linearly, without any visible change in the slope for the whole investigated loading range, up to 3 MW/m^2 . This means that, for this case, there is no change in the boiling regime.

An extra test for HPEE-1 containing 4-mL water (filling ratio 5.3%) is applied with finer resolution of heat flux data points below 0.1 MW/m^2 . $\Delta T_{\text{wall-HP04}}$ increases linearly at first but with high relative uncertainty of 35%. Then, it moved from $16 \text{ °C} \pm 2.9 \text{ °C}$ to $9 \text{ °C} \pm 2.3 \text{ °C}$ with relative uncertainty of 20% at 0.1 MW/m^2 and increased linearly, overlapping the boiling curves of HPEE-1 with 2.0-mL liquid inside. The decrease of $\Delta T_{\text{wall-HP04}}$ at 0.1 MW/m^2 indicates a change in heat transmission mode from low conduction of the envelope and evaporation at the free surface of a liquid-saturated layer to a capillary-fed boiling in the sintered porous with higher effective heat conductivity [16], as shown in Fig. 6. It means that 4.0-mL liquid is too much for HPEE, especially below 0.1 MW/m^2 . The capillary-fed boiling is not activated, and the liquid will accumulate over the porous structure, increasing the temperature gradient. As the liquid in porous is still cold, the formation of the bubbles is delayed.

A finer resolution of heat flux data points was applied on HPEE-2 with 1.5-mL liquid from a low heat load of 0.04 MW/m^2 . As shown in Fig. 5(b), the boiling curve increased linearly with a lower $\Delta T_{\text{wall-HP04}}$ up to $7 \text{ °C} \pm 1.6 \text{ °C}$ at 0.2 MW/m^2 . Then, the $\Delta T_{\text{wall-HP04}}$ shifted from $10 \text{ °C} \pm 2.9 \text{ °C}$ to $35 \text{ °C} \pm 2.4 \text{ °C}$ at 0.5 MW/m^2 . Around 1 MW/m^2 , $\Delta T_{\text{wall-HP04}}$ shifted back from

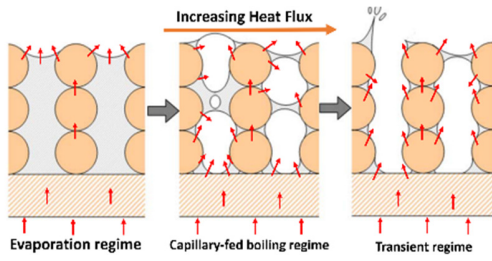


Fig. 6. Schematic illustrations of the two-phase regimes with increased heat flux visualized [16].

$60\text{ }^{\circ}\text{C} \pm 1.6\text{ }^{\circ}\text{C}$ to $48\text{ }^{\circ}\text{C} \pm 2.1\text{ }^{\circ}\text{C}$. The behavior above can be explained by the fact that during the low and medium heat flux, heat transfer mechanism of the porous channels is dominated by the capillary-fed boiling mode. The channels providing a lower resistance path for the vapor to escape [17], allowing the larger bubbles go out and the capillary force on the channels drive more liquid flows to the evaporator. When heat flux is 1 MW/m^2 , the vapor bubbles are more produced and move rather quickly, flushing in the channels, changing the heat transfer mechanism to the convection boiling mode [10], [18], increasing the heat transfer capability. After 1 MW/m^2 , $\Delta T_{\text{wall-HP04}}$ increased quickly again but heat flux changed little, indicating the reduce of the heat transfer capability. At 2.2 MW/m^2 , the superheat of HPEE-2 is $118\text{ }^{\circ}\text{C} \pm 6.4\text{ }^{\circ}\text{C}$. At the same heat flux, $\Delta T_{\text{wall-HP04}}$ of HPEE-2 is lower than HPEE-1.

For a liquid inventory of 1.7 mL , the superheat $\Delta T_{\text{wall-HP04}}$ of HPEE-2 became gentle after 2.8 MW/m^2 . The boiling curve of HPEE-2 with 2.0-mL water has almost the same linear trend as for 1.7 mL but can increase linearly until 3.5 MW/m^2 . It is higher than HPEE-1 with 2.0-mL working fluid, because at the same heat flux, $\Delta T_{\text{wall-HP04}}$ of HPEE-2 is lower than one of HPEE-1. It indicates that the evaporator of HPEE-2 performs better, because the bubbles in evaporator porous structure with channels come out easier than normal porous plate, leaving more space for condensed liquid flows back. Meanwhile, HPEE-2 has lower effective heat resistance of evaporator than HPEE-1, since the average porous thickness is reduced. There is no experiment for HPEE-2 with 4.0-mL fluid, because the extra liquid covers the porous surface, resulting the same pool boiling behavior in the low heat flux range.

To summarize, it can be concluded that the HPEE-1 with 1.5-mL liquid was already in the capillary-fed boiling regime when the heat flux was around 0.2 MW/m^2 (at 0.04 MW/m^2 for HPEE-2 with 1.5 mL). The boiling curves of HPEE-2 shift more obviously to the right at 0.4 MW/m^2 , and it indicates that the regime changed to transient boiling because 1.5 mL of liquid was insufficient to be condensed and flow back to the evaporator. The boiling curve of HPEE-2 of 1.5 mL turning back to the left at 1 MW/m^2 is influenced by the channels on porous, making the heat transfer mechanism switch to the convection boiling mode. When applied heat flux is increased continually, the convection boiling mode changes to transient boiling regime as well, because of the lack of the liquid. The boiling curves of both HPEEs with liquid inventories 1.7 and 2.0 mL increase linearly with heat flux up to 2.5 MW/m^2 , because the condensed water is enough to flow back to the evaporator, making it stay in capillary-fed boiling regime.

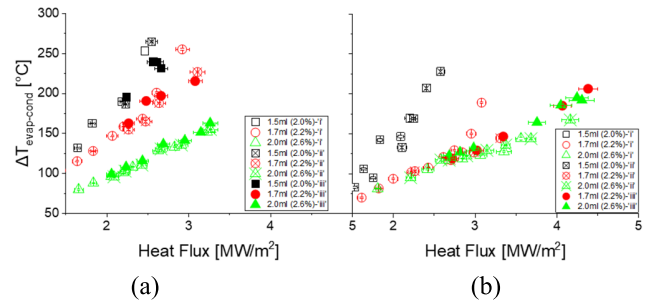


Fig. 7. Difference between the evaporator and condenser temperature with different liquid inventories and flow rates as a function of the heat flux. (a) HPEE-1 and (b) HPEE-2.

From the comparisons above, HPEE-2 with channels on porous evaporator has always better performance than HPEE-1 because the channels provide a low resistance path for the vapor to escape and improve the heat transfer capability at high heat flux with the convection boiling mode. Among them, HPEE-2 with 2.0 mL has the best heat transfer capability.

B. Influence of the Heat Sinks Flow Rates

The temperature measurements of two HPEEs with different liquid inventories were investigated under a constant heat sink flow rate of 90 L/h , introduced as level “1.” At high heat flux, the boiling regime changed easily, and heat transfer capability was limited. However, these operating cases were characterized by an increased condenser temperature and, consequently, a higher vapor temperature. To understand the effects of the condenser, as well as the heat sink’s heat transfer capability, on the performances of the evaporator, the HPEEs are investigated by varying the flow conditions, as mentioned in Section II-D. Since the high heat flux is mainly interested, the experiments start from a heat flux of 2.0 MW/m^2 .

Fig. 7 shows the temperature difference between evaporator and condenser $\Delta T_{\text{evap-cond}}$ versus the heat flux of two HPEEs with different liquid inventories, when the flow rates of the heat sink change. It indicates that the heat sink flow rate has little impact on the temperature difference.

Either working with a fixed coolant temperature rise “2” or a fixed condenser temperature “3,” both heat pipes showed a stable behavior at a higher heat flux. In Fig. 7(b), the results of HPEE-2 with 2.0-mL water even extended to a heat flux as high as 4.3 MW/m^2 when the flow rates maintained the condenser at a specific temperature. It did not show a deterioration of its heat transport capabilities as it can be seen when heat flux increases and cooled at constant flow rate (90 L/h), showing the potential to have higher operating limits. This could be explained by the fact that the vapor temperature increases little with coolant “3” than with coolants “1” and “2” at the same heat flux, requiring lower mass flow.

Unfortunately, it was not possible to access higher heat flux with the existing experimental setup due to the temperature limitations of the electrical heater. Hence, it is not an easy way to identify which case would perform better.

Then, the flow rate’s influence on the heat transfer characteristic of the evaporator $\text{HTCH}_{\text{evap}}$ is looked into detail with a function of the heat flux, as shown in Fig. 8. It indicates that higher flow rate “2” has no evident positive influence on the

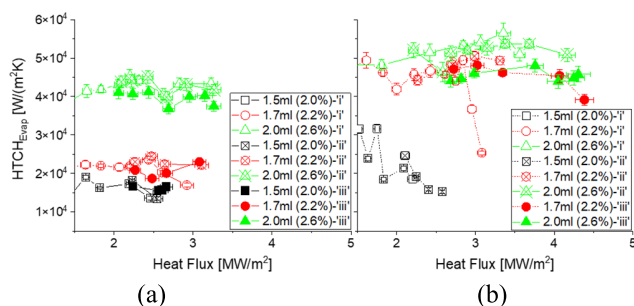


Fig. 8. Heat transfer characteristic of the evaporator $HTCH_{evap}$ with different liquid inventories and flow rates as a function of the heat flux. (a) HPEE-1 and (b) HPEE-2.

$HTCH_{evap}$ for both HPEEs with different liquid inventories. The heat transfer characteristic $HTCH_{evap}$ with flow rate “3” even shows a decreased value.

This can be explained by the function of $HTCH_{evap} = (Q/\Delta T_{wall-HP04})$. As the high heat sink flow rates applied on the condenser directly, the condenser and vapor temperatures decrease more noticeably than the evaporator temperature. As a result, when the flow rate increases, the difference $\Delta T_{wall-HP04}$ between the evaporator and vapor temperature grows, diminishing the heat transfer characteristic $HTCH_{evap}$. However, even the evaporator temperature decreases less than vapor and condenser temperature when flow rate increases, the reduced evaporator temperature can avoid the heater reach its temperature limitation quickly and help the experiments go further to higher heat flux.

IV. CONCLUSION

Due to the temperature limitation of the electric copper heater, the experiment of HPEE-2 with 2.0-mL liquid inside was tested up to 4.3 MW/m². However, the results are already close to the value tested by Weibel [16].

Among three liquid inventories, 1.5, 1.7, and 2.0 mL (corresponding to 2%, 2.2%, and 2.6% of vapor space), the HPEEs with 2.0 mL performed better than others. The results of HPEE-1 with 4.0-mL liquid (5.3% of vapor space) show almost the same performance as HPEE-1 with 2.0-mL liquid inside. However, too much liquid needs more heat flux to start the capillary-fed boiling. At low heat flux (below 0.1 MW/m²), the liquid only accumulates over the capillary structure, resulting in pool boiling and reducing the heat transfer capability.

The impact of the heat sink flow rate on the mock-up operation is observed only for the mock-up HPEE-2 featuring an evaporator with a profiled surface, and the influence becomes significant mainly at high heat loads.

In general, the results of HPEE-2 with channels on the evaporator’s surface indicate a better performance than HPEE-1. It performs well up to 4.3 MW/m² when equipped with 2.0 mL of working fluids and cooled by flow rate “2,” which is adjusted to control temperature differential at 8 °C. The limitations of the experimental setup restricted the exploration of a wider operating space; however, the results indicate that the current limit (of 4.3 MW/m²) could be pushed further up, as there is no sign of dry-out. Taking into account that the mock-up uses bronze instead of copper for the sintered porous, it is expected that a copper-based evaporator would perform better than the presented one with bronze due to the higher heat conductivity of the meta.

ACKNOWLEDGMENT

Views and opinions expressed are, however, those of the author(s) only and do not necessarily reflect those of the European Union or the European Commission. Neither the European Union nor the European Commission can be held responsible for them.

REFERENCES

- [1] J. H. You et al., “Divertor of the European DEMO: Engineering and technologies for power exhaust,” *Fusion Eng. Des.*, vol. 175, Feb. 2022, Art. no. 113010, doi: [10.1016/j.fusengdes.2022.113010](https://doi.org/10.1016/j.fusengdes.2022.113010).
- [2] G. A. Carlson and M. A. Hoffman, “Heat pipes in the magnetic-field environment of a fusion reactor,” *J. Heat Transf.*, vol. 94, no. 3, pp. 282–288, Aug. 1972, doi: [10.1115/1.3449933](https://doi.org/10.1115/1.3449933).
- [3] N. L. Schwartz and M. A. Hoffman, “A heat pipe concept for cooling a liquid-pool blanket of a tandem mirror fusion reactor,” *Nucl. Technol.-Fusion*, vol. 4, no. 3, pp. 479–490, Nov. 1983, doi: [10.13182/fst83-a22797](https://doi.org/10.13182/fst83-a22797).
- [4] V. Kovalenko, V. Khripunov, A. Antipenkov, and A. Ulianov, “Heat-pipes-based first wall,” *Fusion Eng. Des.*, vol. 27, pp. 544–549, Mar. 1995, doi: [10.1016/0920-3796\(95\)90170-1](https://doi.org/10.1016/0920-3796(95)90170-1).
- [5] A. Makhankov et al., “Liquid metal heat pipes for fusion application,” *Fusion Eng. Des.*, vol. 42, nos. 1–4, pp. 373–379, Sep. 1998, doi: [10.1016/s0920-3796\(98\)00216-6](https://doi.org/10.1016/s0920-3796(98)00216-6).
- [6] J. Rosenfeld and J. Lindemuth, “Evaluation of porous media heat exchangers for plasma facing components,” in *Proc. Symp. Fusion Eng.*, vol. 2, 1993, pp. 1210–1213, doi: [10.1109/fusion.1993.518540](https://doi.org/10.1109/fusion.1993.518540).
- [7] W. Wen, B.-E. Ghidersa, W. Hering, J. Starflinger, and R. Stieglitz, “Heat pipe technology based divertor plasma facing component concept for European DEMO,” *Fusion Eng. Des.*, vol. 164, Mar. 2021, Art. no. 112184, doi: [10.1016/j.fusengdes.2020.112184](https://doi.org/10.1016/j.fusengdes.2020.112184).
- [8] N. H. Afgan, L. A. Jovic, S. A. Kovalev, and V. A. Lenykov, “Boiling heat transfer from surfaces with porous layers,” *Int. J. Heat Mass Transf.*, vol. 28, no. 2, pp. 415–422, Feb. 1985, doi: [10.1016/0017-9310\(85\)90074-2](https://doi.org/10.1016/0017-9310(85)90074-2).
- [9] W. Wen, B.-E. Ghidersa, W. Hering, J. Starflinger, and R. Stieglitz, “Heat pipe-based DEMO divertor target concept: High heat flux performance evaluation,” *J. Nucl. Eng.*, vol. 4, no. 1, pp. 278–296, Mar. 2023, doi: [10.3390/jne4010021](https://doi.org/10.3390/jne4010021).
- [10] D. Zhang et al., “Boiling heat transfer performance of parallel porous microchannels,” *Energies*, vol. 13, no. 11, p. 2970, Jun. 2020, doi: [10.3390/en13112970](https://doi.org/10.3390/en13112970).
- [11] H.-J. Kretzschmar and W. Wagner, *International Steam Tables*, 3rd ed. Berlin, Germany: Springer, 2019.
- [12] *Guide to the Expression of Uncertainty in Measurement—Part 6: Developing and Using Measurement Models*, Standard JCGM106, Int. Organ. Stand. Geneva, JCGM, GUM-6, 2020. [Online]. Available: <https://www.bipm.org/en/publications/guides>
- [13] V. Guichet and H. Jouhara, “Condensation, evaporation and boiling of falling films in wickless heat pipes (two-phase closed thermosyphons): A critical review of correlations,” *Int. J. Thermofluids*, vols. 1–2, Feb. 2020, Art. no. 100001, doi: [10.1016/j.ijft.2019.100001](https://doi.org/10.1016/j.ijft.2019.100001).
- [14] K. Baraya, J. A. Weibel, and S. V. Garimella, “Heat pipe dryout and temperature hysteresis in response to transient heat pulses exceeding the capillary limit,” *Int. J. Heat Mass Transf.*, vol. 148, Feb. 2020, Art. no. 119135, doi: [10.1016/j.ijheatmasstransfer.2019.119135](https://doi.org/10.1016/j.ijheatmasstransfer.2019.119135).
- [15] V. P. Carey, *Liquid Vapor Phase Change Phenomena: An Introduction to the Thermophysics of Vaporization and Condensation Processes in Heat Transfer Equipment*, 2nd ed. New York, NY, USA: Taylor & Francis, 2007.
- [16] J. A. Weibel and S. V. Garimella, “Recent advances in vapor chamber transport characterization for high-heat-flux applications,” *Adv. Heat Transf.*, vol. 45, pp. 209–301, Jan. 2013, doi: [10.1016/B978-0-12-407819-2.00004-9](https://doi.org/10.1016/B978-0-12-407819-2.00004-9).
- [17] M. P. Mughal and O. A. Plumb, “An experimental study of boiling on a wicked surface,” *Int. J. Heat Mass Transf.*, vol. 39, no. 4, pp. 771–777, Mar. 1996.
- [18] Z. G. Qu, Z. G. Xu, C. Y. Zhao, and W. Q. Tao, “Experimental study of pool boiling heat transfer on horizontal metallic foam surface with crossing and single-directional V-shaped groove in saturated water,” *Int. J. Multiphase Flow*, vol. 41, pp. 44–55, May 2012, doi: [10.1016/j.ijmultiphaseflow.2011.12.007](https://doi.org/10.1016/j.ijmultiphaseflow.2011.12.007).